Directional assembly of polyaniline functionalized gold nanoparticles



2007 J. Phys.: Condens. Matter 19 196225

(http://iopscience.iop.org/0953-8984/19/19/196225)

IOP PUBLISHING JOURNAL OF PHYSICS: CONDENSED MATTER

J. Phys.: Condens. Matter **19** (2007) 196225 (8pp) doi:10.1088/0953-8984/19/19/196225

# Directional assembly of polyaniline functionalized gold nanoparticles

**Kaushik Mallick**[1], **Mike J Witcomb**[2] **and Mike S Scurrell**[1]

[1] Molecular Sciences Institute, University of the Witwatersrand, Johannesburg, Private Bag 3, WITS 2050, South Africa
[2] Electron Microscope Unit, University of the Witwatersrand, Johannesburg, Private Bag 3, WITS 2050, South Africa

E-mail: kaushik.mallick@mailcity.com

Received 19 December 2006, in final form 29 January 2007
Published 20 April 2007
Online at stacks.iop.org/JPhysCM/19/196225

**Abstract**

Polyaniline encapsulated and functionalized self-assembled gold nanoparticles have been synthesized using an interfacial polymerization approach. The polyaniline and gold nanoparticles were formed at the aqueous and organic interface and a directional growth of the self-assembled gold nanoparticles was observed. The resultant composite material was characterized by means of different techniques. IR, Raman and UV–visible (UV–vis) spectra provided information on the chemical structure of the polymer. UV–vis spectrum also indicated the functionalization of the gold nanoparticles by the polymer. TEM images showed the morphology of the polymer and the metal particles.

(Some figures in this article are in colour only in the electronic version)

## 1. Introduction

Self-assembly of nanoparticles mediated by polymers provides access to stabilized metals [1] and semiconductors [2] as well as allowing for the fabrication of new structured nanoscale materials [3]. Several attributes of the individual building blocks such as the size and shape of individual metal particles, composition of the monolayer and functional groups on the polymers permits control over the structure of these nanocomposites. Incorporation of metal nanoparticles into the polymer matrix is a field of particular interest for materials engineering and for the study of nanoparticle–matrix interactions [4]. Although there are many complexes of ligand-stabilized metal nanoparticles, there are few examples of polymer stabilized metal nanoparticles in which the metal nanoparticles are functionalized by the polymer [5].

There have been a variety of attempts to make nanoparticle–polymer composites. Overall, we note four different approaches used to date. The first technique comprises the preparation of metal nanoparticles in the polymer matrix by the reduction of metal salts in the polymer

matrix [6]. The second technique consists of polymerizing the organic monomer around the preformed metal nanoparticles [7]. The third approach has involved the blending of preformed nanoparticles into a pre-synthesized polymer [8]. The fourth procedure is the most desirable approach in order to achieve an intimate contact between the metal and the polymer, and it involves the blending of a monomer and a metal salt [9]. The choice of the metal salt and the monomer should be such that the metal salt can oxidize the monomer to form a polymer as well as utilize the electrons released during the oxidation to reduce the metal salt to form metal nanoparticles. Results from our laboratory have reported that polyaniline and derivatives of polyaniline form metal–polymer composite materials with gold, copper and palladium [10–13].

The aim of the present study was to determine whether the polymer acts as largely an inert matrix carrying the metal nanoparticle or whether the metal nanoparticle is functionalized by the polymer. In this experiment, we have used the gold–polyaniline system due to the well defined plasmon absorption band of the gold nanoparticles in the visible region and the well established size dependence of the position of the band [14]. When the polyaniline concentration is high, the plasmon absorption band of the gold nanoparticles overlaps with the benzenoid to quinonoid excitonic transition of the polymer and covers the whole visible region from 500 to 900 nm with an absorption peak at 770 nm [15].

The strategy followed consisted of growing a high concentration of gold nanoparticles with the simultaneous attachment of a thin polyaniline layer. In order to achieve such a condition, we allowed the particles and the polymer to grow at the interface of an organic and aqueous layer by using the concept of interfacial polymerization [16].

## 2. Experimental section

Aniline was purchased from BDH (London) and distilled at a reduced pressure over zinc metal. The middle fraction was collected and stored at $-10\,^{\circ}$C under argon. We received toluene from MERCK and it was utilized without further purification. $HAuCl_4$ was purchased from Aldrich. Crystalline $HAuCl_4$ was dissolved in ultra-pure water and made to a stock solution having a concentration of $10^{-2}$ mol dm$^{-3}$.

In a typical reaction, 0.05 g of aniline was diluted in 10 ml of toluene in a 25 ml conical flask. An aqueous solution of hydrogen tetrachloroaurate (5 ml, $1 \times 10^{-2}$ mol dm$^{-3}$) was added dropwise to the solution of diluted aniline in a static environment. A 'ruby red' coloured thin layer was deposited at the bottom of the pot. The material was allowed to settle for 10 min. After that 5 $\mu$l of the final colloidal solution, taken from the bottom of the conical flask, was pipetted onto lacey, carbon coated, copper TEM grids for TEM study. The remaining portion of the compound was used for UV–vis, IR and Raman analyses. The whole process was carried out at room temperature.

Transmission electron microscopy studies of the particles were carried out at an accelerating voltage of 197 kV using a Philips CM200 TEM equipped with a $LaB_6$ source. An ultra-thin windowed energy dispersive x-ray spectrometer and a Gatan Model 678 Imaging Filter (GIF) attached to the TEM were used to determine the chemical composition of the samples.

For UV–vis spectra analysis, a small portion of the solid sample was dissolved in methanol and scanned within the range 300–1000 nm, using a Varian, CARY, 1E, digital spectrophotometer.

Raman spectra were acquired using the green (514.5 nm) line of an argon ion laser as the excitation source. Light dispersion was undertaken via the single spectrograph stage of a Jobin–Yvon T64000 Raman spectrometer. Power at the sample was kept very low (0.73 mW), while the laser beam diameter at the sample was $\sim$1 $\mu$m.

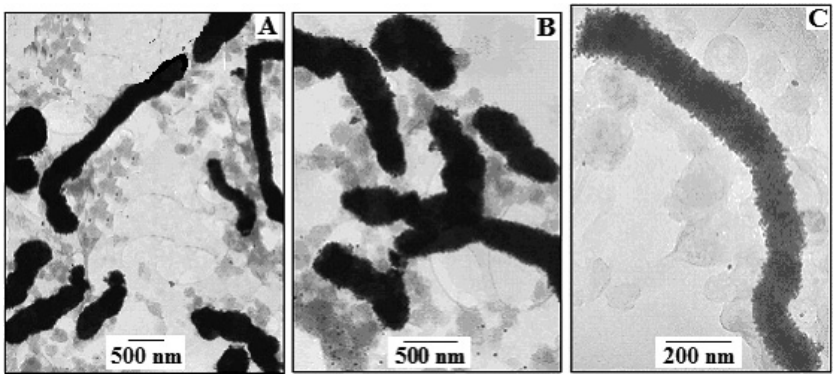


**Figure 1.** TEM images showing the directional growth of the self assembled gold particles ((A) and (B)). (C) is a magnified TEM image showing the fibre-like morphology.

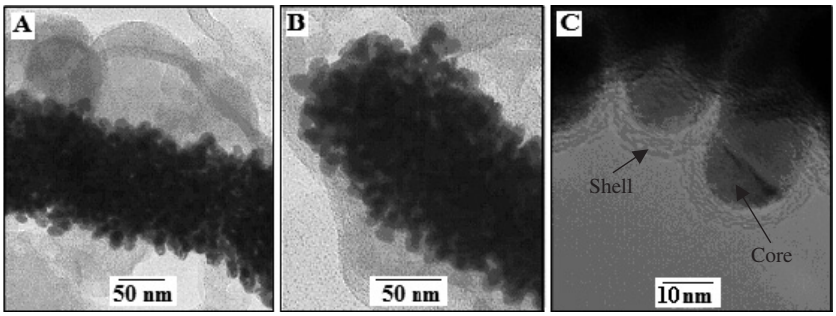


**Figure 2.** Higher magnification TEM images ((A) and (B)) of parts of the area in figure 1(C) reveal that the fibre-like morphology comprised a self-assembly of individual gold nanoparticles, (C) indicates that the gold nanoparticles are covered with polyaniline and form a $\text{core}_{\text{gold}}$–$\text{shell}_{\text{polymer}}$ type structure.

A Perkin-Elmer 2000 FT-IR spectrometer, operating within the range 850–4000 $\text{cm}^{-1}$ with a resolution 4 $\text{cm}^{-1}$, was used for the infrared spectra analyses. For this study, one drop of diluted composite material was deposited in the form of a thin film onto the NaCl disc.

## 3. Results and discussion

### *3.1. Transmission electron microscopy study*

Figures 1(A) and (B) are low magnification TEM images of the product collected from the bottom of the reaction pot. Figure 1(C) is the magnified TEM image showing the fibre-like morphology. Further magnified TEM images (figures 2(A) and (B)) of part of figure 1(C) reveal that the fibre-like morphology is composed of an assembly of individual particles. Stacking faults which were generated during the gold particle growth process could be seen in some of the nanoparticles e.g. figure 2(C). Such planar faults exist when two adjacent atomic planes are not in their correct crystallographic registry. For example, a face centred cubic (fcc) crystal is built by stacking (111) planes in the sequence ABCABC. Errors in this stacking sequence such as ABCBCABC create a discontinuity or fault. These have been seen in chemically synthesized fcc nanocrystals such as nickel [17], silver [18] and gold [3].

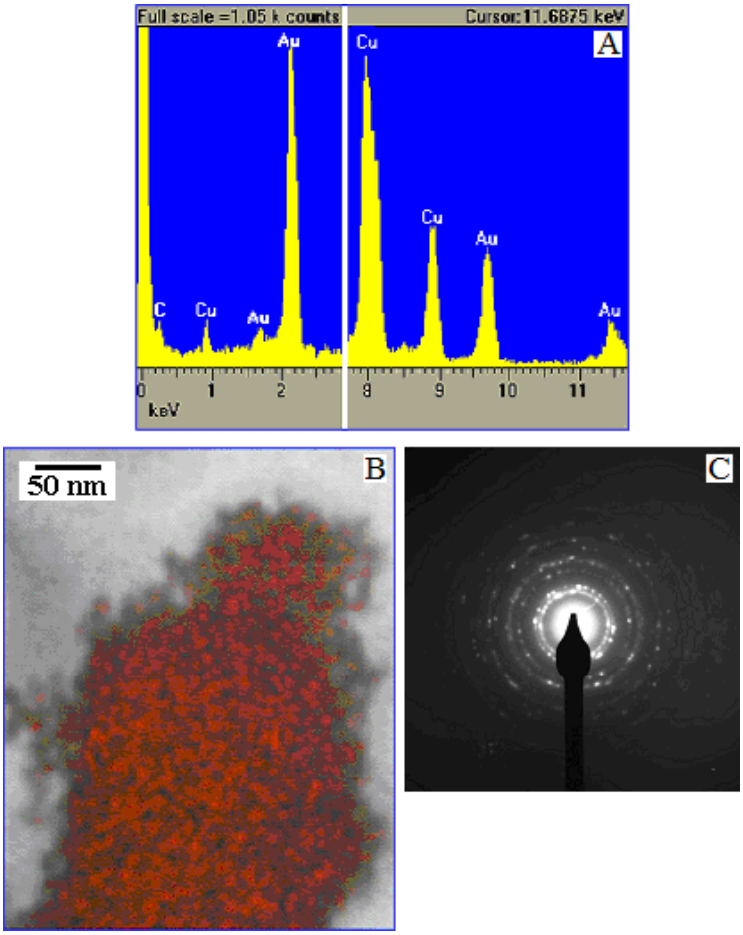


**Figure 3.** (A) EDX spectra from a cluster of nanoparticles. The copper peaks originate from the copper support grid. (B) Elemental mapping utilizing the Au M$\alpha$ x-ray peak confirmed that gold is located only at the nanoparticles. (C) Selected area diffraction patterns obtained from different groups of nanoparticles always yielded a characteristic polycrystalline ring pattern for a face centred cubic structure, the lattice parameter corresponding to that of gold.

*3.1.1. Energy dispersive x-ray (EDX) spectra analysis.* EDX spectra from both single nanoparticles and nanoparticle clusters revealed only the presence of gold, the copper peaks originating from electron scattering onto the copper support grid (figure 3(A)). Elemental mapping utilizing the Au M$\alpha$ x-ray peak confirmed gold to be located only at the nanoparticles (figure 3(B)).

*3.1.2. Selected area diffraction (SAD) pattern analysis.* SAD patterns (figure 3(C)) obtained from different groups of nanoparticles always yielded a characteristic polycrystalline ring pattern for a fcc structure. The lattice parameter was determined to be $0.4086 \pm 0.0011$ nm, a value which corresponds to that of gold [19].

*3.1.3. Electron energy loss spectroscopy (EELS) analysis.* EELS mapping for the Au particle distribution provided unambiguous confirmation that the dark spots are gold. This is most

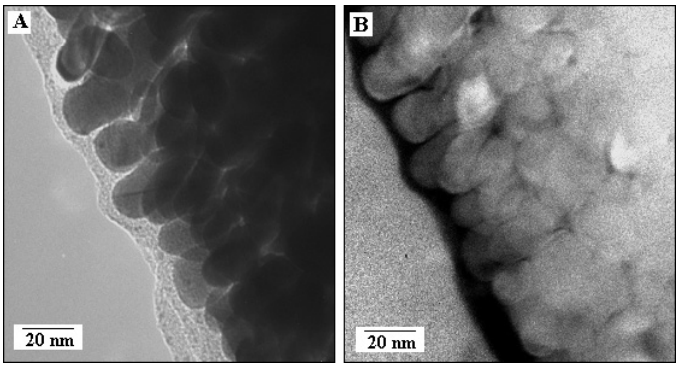


**Figure 4.** (A) Zero-loss image of a polyaniline encapsulated self-assembly of gold particles. (B) Au $O_{2,3}$ edge jump-ratio image of the area shown in (A). All of the dark regions in (A) can clearly be identified as gold nanoparticles.

clearly illustrated in figure 4 where the terminal particles were not overlapping. Figure 4(A) is a zero-loss image. This is an energy filtered image such that it is only derived from electrons which have retained the beam energy when passing through a thin sample. This image contains no useful micro-analytical information. In contrast, figure 4(B) is a gold map from the same region. This Au jump-ratio image was obtained by dividing the Au $O_{2,3}$ post-edge loss image (an image derived from the signal from an energy window placed just above the ionization energy of Au $O_{2,3}$ shell x-rays, the signal being the sum of the background signal at this position which contains no micro-analytical information, and the signal resulting from electrons that lost energy by generating Au $O_{2,3}$ shell x-rays) by the pre-edge image (an image derived from the signal from an energy window placed just before the ionization energy of Au $O_{2,3}$ shell x-rays, this image being a background image). By comparing the zero-loss and jump-ratio images, it can be seen that the dark areas in figure 4(A) correspond to all of the Au particles mapped in figure 4(B). This result was also found for the other areas studied.

### *3.2. Optical characterization*

The optical behaviour of the resultant material was determined by FTIR and Raman spectroscopic analyses.

*3.2.1. Fourier transform infrared study.* In the FTIR spectrum (figure 5), the two peaks at 1595 and 1505 $cm^{-1}$ correspond to the stretching deformations of quinine and benzene rings. The absorption peak at 1300 $cm^{-1}$ corresponds to the C–N stretching mode, while the peak positioned at 1245 $cm^{-1}$ is related to the protonated C–N group. The aromatic C–H in-plane bending mode was observed in the 1245–1045 $cm^{-1}$ region. The out-of-plane deformations of the 1,4 di-substituted benzene rings are located at 870 $cm^{-1}$. This study indicates that the polyaniline is present neither in the fully oxidized nor the fully reduced form due to the presence of both the quinoid and the benzoid forms of structure.

*3.2.2. Raman spectra analysis.* In the Raman spectrum (figure 6), the C–H benzene deformation modes at 1165 $cm^{-1}$ indicate the presence of quinoid rings. The band at 1460 $cm^{-1}$ corresponds to the C=N stretching mode of the quinoid units. The C–N stretching mode of single bonds is in evidence at 1220 $cm^{-1}$, while the band at 1245 $cm^{-1}$ can be assigned to the C–N stretching mode of the polaronic units. The absorption bands at 1350 and 1375 $cm^{-1}$ correspond to the $C–N^{\bullet+}$ stretching modes of the delocalized polaronic charge carrier, the high intensity of the peaks confirming the presence of a high concentration of these forms in the compound. The absorption peak at 1535 $cm^{-1}$ corresponds to the N–H bending deformation

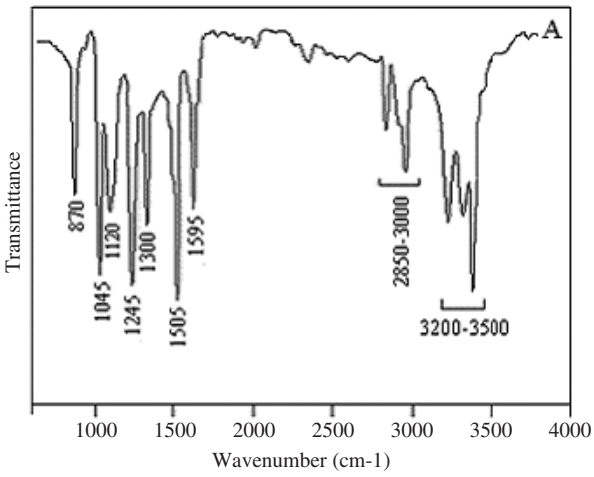


**Figure 5.** Fourier transform IR spectrum of the resultant composite material.

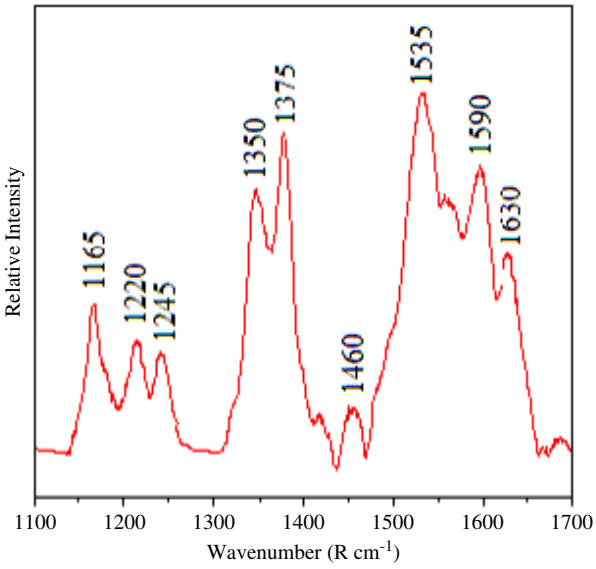


**Figure 6.** Raman spectrum of the composite compound.

band of protonated amine. The C–C deformation bands of the benzenoid ring positioned at 1630 and 1590 $cm^{-1}$ are characteristic of the semiquinone rings.

The spectroscopic data confirmed the formation of polyaniline and from the TEM images, figures 4(A) and (B), it is clear that the gold nanoparticles are covered with polyaniline and form a $core_{gold} - shell_{polymer}$ type structure (figure 2(C)).

*3.2.3. UV–visible spectra study.* Further optical behaviour of the compound is illustrated from the results of UV–vis spectra analysis. The UV–vis spectrum (figure 7) shows three absorption bands at 320, 415 and 550 nm. The absorption peak at 320 nm is due to the $\pi$–$\pi^*$ transition of the benzenoid rings, whereas the peak at 415 nm is due to the polaron/bipolaron transition. When the polyaniline concentration is high, the benzenoid to quinoid excitonic transition covers the whole range from 500 to 900 nm with an absorption peak at 770 nm [15]. However, in the present case, the excitonic transition has been suppressed by the plasmon absorption

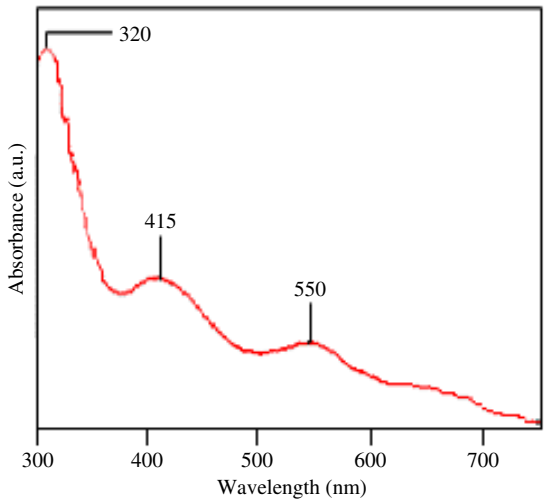


**Figure 7.** UV–visible spectrum of the polyaniline encapsulated gold nanoparticles.

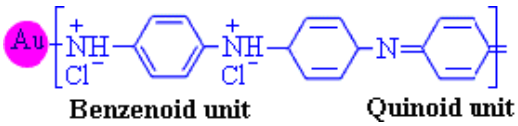


**Figure 8.** Schematic diagram of the polyaniline functionalized gold nanoparticles (GNP).

band of the gold nanoparticles at 550 nm due to the presence of the high concentration of gold particles. The gold nanoparticles, 5–50 nm in size, show a sharp absorption band in the 520–530 nm region due to the collective oscillation of conduction electrons in response to optical excitation [20]. As the particles grow, the absorption band broadens and covers the visible range [21]. Small metal particles, especially gold, have a high electron affinity and can strip off electrons from the surrounding matrix [22]. These charged particles are stabilized by the matrix and the repulsive force between the charged particles then prevents their aggregation [23]. A process of forming such a complex will alter the electron density of the nanoparticle surface. This then directly affects the surface plasmon absorption band which results in a bathochromic shift of 20–30 nm. Such a shift was observed for the polyaniline encapsulated gold nanoparticles and this leads to the conclusion that functionalization of the gold nanoparticles by the polyaniline has taken place. The polyaniline matrix acts as counter ions that stabilize the negatively charged gold particles and prevent agglomeration. The functionalization of the gold particles is through the unit positively charged nitrogen atom of the polyaniline (emaraldine salt) as illustrated in figure 8.

## 4. Mechanistic approach

The mechanism of formation of the gold nanoparticles and the polyaniline is as follows. During the addition of $HAuCl_4$ to aniline, the $HAuCl_4$ acts in a dual role. Firstly, $HAuCl_4$ protonates the aniline to form anilinium cations ($PhNH_3^+$). Secondly, $[AuCl_4]^-$ acts as the oxidizing agent [24, 25] that can oxidize $PhNH_3^+$ and form polyaniline. During polymerization, each step involves the release of an electron [10] and that free electron is then used to reduce the $[AuCl_4]^-$ to form gold atoms. The coalescence of these gold atoms ultimately forms gold nanoparticles, which are encapsulated by the polymer. Since we employed the interfacial polymerization approach in this experiment, polyaniline and gold nanoparticles were formed at the organic

and aqueous interface with a directional orientation of the self-assembled gold nanoparticles encapsulated by polyaniline.

## 5. Conclusions

By applying the concept of interfacial polymerization, we have successfully synthesized polyaniline encapsulated gold nanoparticles. An interfacial polymerization process has allowed the formation of a metal–polymer composite that resulted in the attachment of gold nanoparticles to the polyaniline matrix with a preferential growth direction of the self-assembled gold nanoparticles. A bathochromic shift of the plasmon resonance band of the gold particles in the UV–vis spectra has clearly indicated that an electron transfer has occurred from the polyaniline to the gold. This transfer made the gold surface richer in electrons, resulting in a functionalization of the gold nanoparticles.

Superstructured nanomaterials such as described here have some novel characteristics such as anisotropic electrical transport and electrorheological properties which are technologically useful in different microelectronic systems. This will be addressed in future publications.

## Acknowledgments

K Mallick gratefully acknowledges the National Research Foundation (SA) and the University of the Witwatersrand for financial support. The authors would like to thank one of the referees for their valuable comments to improve this paper.

## References

[1] Mallick K, Witcomb M J and Scurrell M S 2005 *Appl. Phys.* A **80** 395
[2] Petit C, Jain T K, Billoudet F and Pileni M P 1994 *Langmuir* **10** 4446
[3] Mallick K, Witcomb M J and Scurrell M S 2005 *Eur. Phys. J: Appl. Phys.* **29** 45
[4] Swami A, Kumar A, Selvakannan P, Mandal S, Pasricha R and Sastry M 2003 *Chem. Mater.* **15** 17
[5] Jordan R, West N, Ulman A, Chou Y-M and Nuyken O 2001 *Macromolecules* **34** 1606
[6] Selvan S T, Spatz J P, Klok H-A and Möller M 1998 *Adv. Mater.* **10** 132
[7] Lee J, Sundar V C, Heine J R, Bawendi M G and Jensen K F 2000 *Adv. Mater.* **12** 1102
[8] Corbierre M K, Cameron N S, Sutton M, Mochrie S G J, Lurio L B, Rühm A and Lennox R B 2001 *J. Am. Chem. Soc.* **123** 10411
[9] Mallick K, Witcomb M J and Scurrell M S 2007 *Phys. Status Solidi* **1** (RRL) R1
[10] Mallick K, Witcomb M J, Dinsmore A and Scurrell M S 2005 *Macromol. Rapid Commun.* **26** 232
[11] Mallick K, Witcomb M J and Scurrell M S 2006 *Eur. Polym. J.* **42** 670
[12] Mallick K, Witcomb M J, Dinsmore A and Scurrell M S 2005 *Langmuir* **21** 7964
[13] Mallick K, Witcomb M J and Scurrell M S 2006 *Eur. Phys. J.* E **19** 149
[14] Kamat P V 2002 *J. Phys. Chem.* B **106** 7729
[15] Wang Y, Liu Z, Han B, Sun Z, Huang Y and Yang G 2005 *Langmuir* **21** 833
[16] Huang J and Kaner R B 2004 *J. Am. Chem. Soc.* **126** 851
[17] Phung X, Groza J, Stach E A, Williams L N and Richey S B 2003 *Mater. Sci. Eng.* A **359** 261
[18] Mallick K, Witcomb M J and Scurrell M S 2004 *J. Mater. Sci.* **39** 4459
[19] Cullity B D 1967 *Elements of X-ray Diffraction* (Reading, MA: Addison-Wesley)
[20] Henglein A and Meisel D 1998 *Langmuir* **14** 7392
[21] Chen S, Ingram R S, Hostetler M J, Pietron J J, Murray R W, Schaaff T G, Khoury J T, Alvarez M M and Whetten R L 1998 *Science* **280** 2098
[22] Furstner A 1995 *Active Metals: Preparation, Characterization, Applications* (New York: Wiley)
[23] Pileni M P 2001 *J. Phys. Chem.* B **105** 3358
[24] Sun X, Dong S and Wang E 2004 *Chem. Commun.* 1188
[25] Mallick K, Witcomb M J and Scurrell M S 2006 *Eur. Phy. J.* E **20** 347